—研究論文—
Scientific Paper

Determination of Sea Ice Concentration from AVHRR Visible and Near Infrared Imagery

Takashi YAMANOUCHI*, Kazuya SUZUKI**, Masatoshi MATSUSHITA***, Masanobu SHIMIZU** and Yasuhiko NAITO*

AVHRR 可視・近赤外画像による海氷密集度の算出

山内　恭*・鈴木一哉**・松下昌寿***・清水正修**・内藤靖彦*

要旨: NOAA 衛星 AVHRR 画像の可視および近赤外のアルベードから，海氷の密集度を求めた．1つの方法では，1つのチャンネルのデータから，開水面のアルベードを密集度 0% に，積雪面のアルベードを密集度 100% に対応するものとし，その間のアルベードに対しては線型補間することによって密集度を出した．この方法によると，表面状態が変化することによるアルベードの変化が，密集度の変化として出てしまう．もう1つの方法では，2つのチャンネルのデータを用い，海氷密集度だけでなく海氷の表面状態をも導出した．この方法では，先の方法による不確定さを少なくすることができる．海氷面状態は「雪による被覆率」として示した．航空写真と衛星データとの比較を試みたが，航空写真は海氷表面状態を調べるのに役立つ．夏の海氷状態，海氷密集度の時間変化を調べた．

Abstract: Sea ice concentrations are determined from the visible and near infrared albedo of the AVHRR imagery. One method uses only one channel data to interpolate the ice concentration between 0 and 100% corresponding to the open water and the snow cover, respectively. This method yieds an uncertainty owing to the variation of albedo by the surface condition change. Another method uses two-channel data to derive not only the ice concentration but also the ice surface condition and can eliminate uncertainties involved in the first method. The ice surface condition is expressed by "snow coverage". Air photographs are compared with the satellite data. They are helpful to discuss the surface condition of sea ice. Time variations of the concentration and surface condition of summer sea ice are discussed.

1. Introduction

The monitoring of sea ice is of great importance for studies of the global climate. Not only the ice edge is the key parameter for the climate but also the amount of open water within the pack ice and the snow cover on the sea ice strongly influence the heat balance (WELLER, 1980; LEDLY, 1985).

Among many methods for sea ice observations, the satellite remote sensing has beome popular in recent years. Time sequence data of visible and infrared imagery

* 国立極地研究所. National Institute of Polar Research, 9–10, Kaga 1-chome, Itabashi-ku, Tokyo 173.
** 電気通信大学. University of Electro-Communications, 5–1, Chofugaoka 1-chome, Chofu-shi, Tokyo 182.
*** 豊島区南長崎 3 丁目 18–15. 18–15 Minami nagasaki 3-chome, Toshima-ku, Tokyo 171.

of meteorological satellite were used to obtain sea ice variations (WENDLER, 1973; DEY, 1980, 1981) and the higher resolution imagery of LANDSAT was used to derive the sea ice concentration (COMISO and ZWALLY, 1982). However, not many works using visible or infrered imagery are concerned with the quantitative study of ice concentration. Recently, microwave data have been proved fruitful to sense not only the concentration but also the state of sea ice (first year ice, multi year ice, . . .).

In the present paper, sea ice surface condition and concentration near Lützow-Holm Bay, Antarctica, are inferred from the NOAA AVHRR (advanced very high resolution radiometer) visible and near-i.r. imagery. The ground surface resolution of AVHRR is lower than that of LANDSAT MSS (mutli spectral scanner) or TM (thematic mapper), and AVHRR data are not very powerful to sense the ice properties and to be used in the cloudy atmosphere as the microwave data (COMISO, 1983; YAMANOUCHI and SEO, 1984). However, AVHRR data have an advantage of frequent acquisition, more than once a day, and have a much higher resolution (order of 1 km) than the microwave data of Nimbus satellites. Not only the concentration but the surface type — snow coverage — are determined at once from the data of visible (channel 1) and near-i.r. (channel 2) imagery of AVHRR. The possibility to obtain sea ice surface condition from the ratio of radiance in two wavelength region, visible and near-i.r., has been reported by GRENFELL and PEROVICH (1984); however, no works were done using the actual satellite data to infer the sea ice condition quantitatively.

2. Methodology

An advanced very high resolution radiometer (AVHRR) of NOAA-7 polar-orbiting satellite scans the surface with $\pm 55^\circ$ width (cross track scan) from about 850 km height and provides five-channel imagery with the ground resolution about 1.1 km at the nadir. Channels 1 (0.58–0.68 μm) and channel 2 (0.725–1.1 μm) measure reflected solar radiation normalized by the solar constant and channels 3 (3.55–3.93 μm), 4 (10.3–11.3 μm) and 5 (11.5–12.5 μm) measure emitted terrestrial radiation including some part of reflected solar radiation which reaches the satellite. In this paper, we use the word "albedo" to indicate the reflectance of channels 1 and 2 measured at the altitude of the satellite.

Owing to the high contrast of albedo between the open water and sea ice, the ice concentration can be derived from albedo measurements. Since the resolution of AVHRR pixel is about 1 km, not all the ice floes or open water are resolved. It is assumed that a pixel with albedo near the water peak in the histogram corresponds to 0% ice cover and that near the ice peak corresponds to 100% ice cover. Albedo values between these two extremes are assigned to intermediate ice-concentration by linear interpolation.

The above method is applicable only to the case when the single value of the albedo corresponds to 100% sea ice. Actually, the surface condition of sea ice is variable and the albedo of 100% ice cannot be uniquely determined.

Albedos of channels 1 (0.58–0.68 μm) and 2 (0.725–1.1 μm) of AVHRR are used to derive the concentration of sea ice and the condition of ice surface. The ratio of each surface type within one target area, x: open water, y: bare ice, z: snow-covered

ice, can be expressed from the albedo in channels 1, a_1, and 2, a_2, as

$$\begin{aligned} &x+y+z=1 \\ &\alpha_1 x+\beta_1 y+\gamma_1 z=a_1 \\ &\alpha_2 x+\beta_2 y+\gamma_2 z=a_2 , \end{aligned} \tag{1}$$

where α_i, β_i and γ_i are the typical albedos for the open water, bare ice and snow-covered ice, and suffixes indicate the channel number, respectively, if the atmospheric effect is negligible.

The spectral albedo depends on the surface condition. The albedo of bare ice is lower than the albedo of dry and clean snow in the total shortwave region and especially lower in the near-i.r. region (channel 2) (WARREN, 1982; GRENFELL and PEROVICH, 1984). So, we can assume as

$$\begin{aligned} &\alpha_1<\beta_1<\gamma_1 , \\ &\alpha_2<\beta_2<\gamma_2 , \\ &\frac{\gamma_1}{\gamma_2}<\frac{\beta_1}{\beta_2} . \end{aligned} \tag{2}$$

The ratio of the albedo in the visible to that in the near-i.r. has an information of the surface condition. We describe the surface condition simply as "the snow coverage of the sea ice surface".

Values of α_i, β_i and γ_i ($i=1, 2$) are determined from pixels of AVHRR imagery, which are assumed to be composed of 100% water, bare ice or snow. $y+z$ indicates the normal "sea ice concentration".

The data of AVHRR were derived from the HRPT tape obtained at Syowa Station and research ship SHIRASE. Since 1980, the HRPT data are received at Syowa Station by the Japanese Antatctic Research Expedition. Also, these data are received on SHIRASE during her voyage near the Antarctic coast. The AVHRR data were extracted from the HRPT data after they were converted into a computer compatible tape at the National Institute of Polar Research. Calibrations and corrections of map projection are made as reported elsewhere. Since the calibrated values a_i' of channels 1 and 2, are the radiance of the reflected solar radiation (I_r) normalized by the solar constant (I_o), the "albedos" defined in the present paper are obtained as follows.

$$\begin{aligned} &a_i'=\frac{I_r}{I_o} \\ &a_i=\frac{I_r}{I_o \cos\theta}=\frac{a_i'}{\cos\theta} \quad (i=1, 2) , \end{aligned} \tag{3}$$

where θ is the solar zenith angle at each target area. There is also other viewing angle and zenith angle dependence of albedo owing to the atmospheric effect or surface properties; however, they are neglected in the present analysis, since the research area is limitted to about 500×500 km (about 10 degrees in longitude and 3 degrees in latitude).

3. Sea Ice Concentration

Figure 1 shows the channel 2 image of AVHRR on January 29, 1984, near Syowa Station and Lützow-Holm Bay including the research area (within the square). Though quantitatively difficult, we can assume the ice condition from this figure. Lützow-Holm Bay is filled with fast ice, some leads are seen within fast ice. The northern part is covered with pack ice, including some large areas of open water.

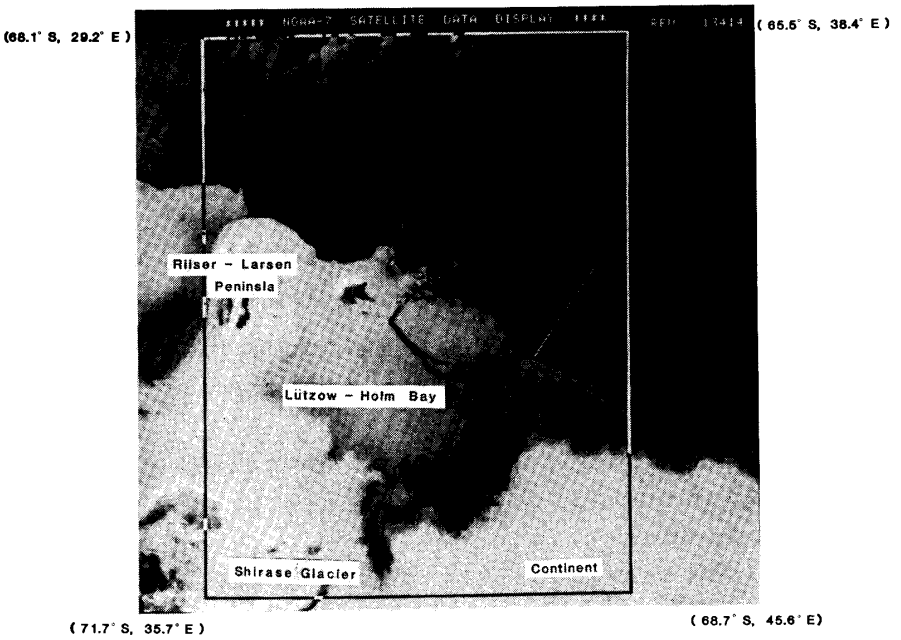

Fig. 1. NOAA-7 AVHRR imagery of channel 2 (0.725–1.1 μm) around Lützow-Holm Bay. Map projection is polar stereo and corner points are 68.1°S, 29.2°E (upper-left), 65.5°S, 38.4°E (upper-right), 71.7°S, 35.7°E (bottom-left) and 68.7°S, 45.6°E (bottom-right), and vertical line is parallel to the 0° meridian. The square in the photograph shows a research area referred to in the following figures, and the dotted line shows a flight line explained in section 4.

3.1. Sea ice concentration from single-channel data

Sea ice concentrations are obtained from the albedo of one channel. Histograms are made for pixels contained in the research area of 352×464 pixels for channels 1 and 2, respectively (Fig. 2). From the histogram of the albedo of channel 1, as shown in Fig. 2a, it is assumed that 5% of albedo (lower peak) corresponds to the open water (0% ice concentration) and 78% of albedo (high peak) to 100% ice concentration. Similar assumption can be made for the histogram of channel 2 (Fig. 2b). Ice concentrations are obtained from the albedo linearly interpolated between these two extremes. The actual calculations are made for the average area composed of 8×8 pixels ($\approx 10 \times 10$ km, hereafter called "frame").

Figure 3 shows the results from channel 1 for the research area which contains 44×58 frames. The ice concentration is indicated by the size of dotted area in each frame, and the size of white area indicates the percentage of open water. Large

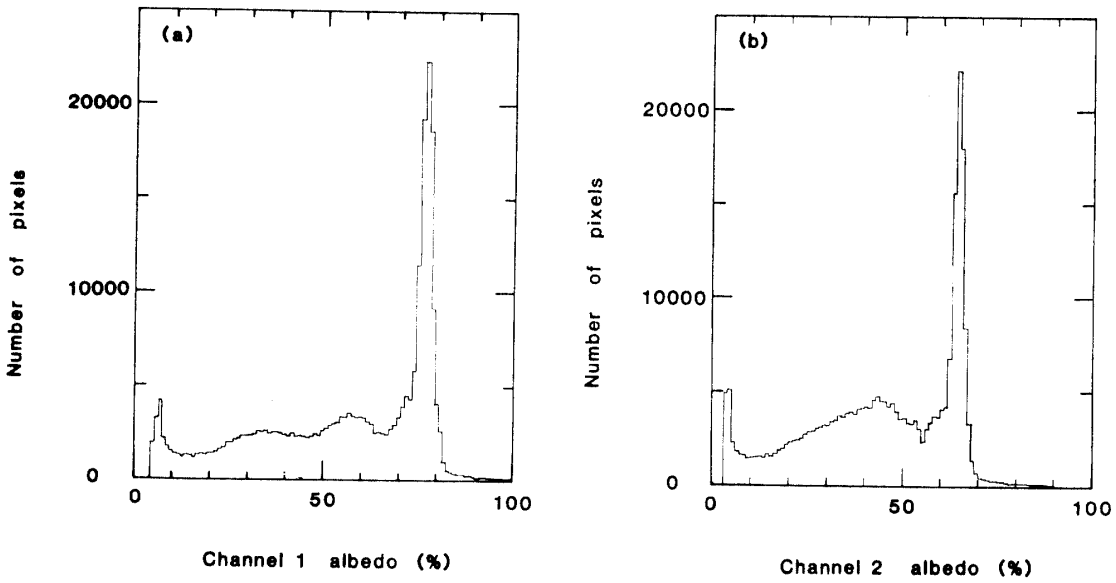

Fig. 2. Histogram of albedo for (a) channel 1 and (b) channel 2 within the research area shown in Fig. 1.

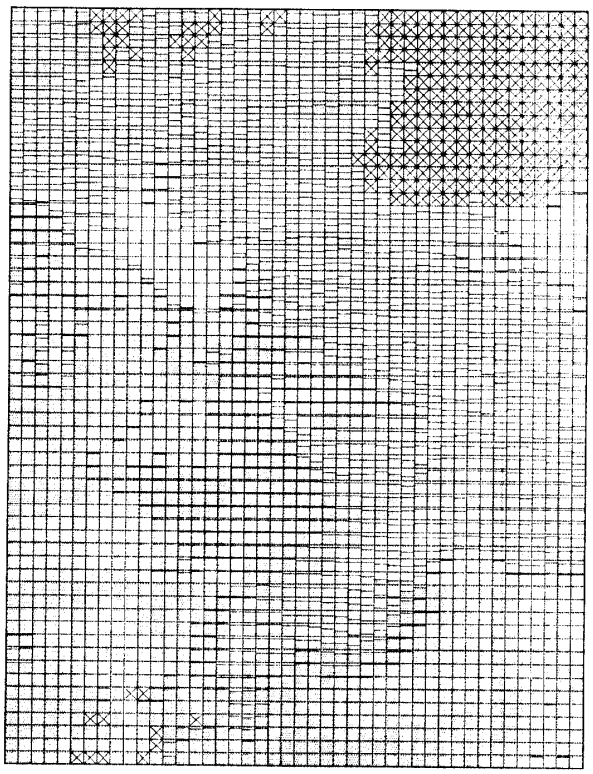

Fig. 3. Sea ice concentration map of the research area. Corner points are 67.8°S, 30.3°E (upper-left), 66.1°S, 36.7°E (upper-right), 71.2°S, 36.6°E (bottom-left) and 69.2°S, 43.4°E (bottom-right). Each frame is composed of 8×8 array (≈10×10 km). Dotted area in each frame indicates sea ice concentration and the cross indicates cloud frame.

polynia is seen in the left upper-middle part of the figure and regions of low ice concentration are distributed in the upper-middle part. Regions of low ice concentration are also distributed in the east side of Lützow-Holm Bay. Most frames for the fast ice in the Bay, some frames on the continental slope and frames around the Shirase Glacier also resulted to contain some open water areas. Cloud areas are indicated by crosses obtained by the method using two-channel data (SUZUKI *et al.*, 1985). It is difficult to originate the threshold to distinguish the cloud from snow or ice using one-channel data.

The indication of open water for the frames on the continental slope or around the Shirase Glacier is suspicious. Local standard deviations for 2×2 array (standard deviations of each pixel from the mean of 2×2) are shown in Fig. 4. The point of low standard deviation corresponds to the area of homogeneous surface and the point of high standard deviation corresponds to the area of variable surface within 2×2 array as in the pack ice composed of mixture of small ice floe and open water. It is clear from this figure that the open water is around 5% albedo. However, points with low standard deviation are distributed between about 55 to 80% albedo, which seem to correspond to the 100% snow or ice cover. From this figure, it is assumed that the continental snow cover and the snow-covered sea ice correspond to the part of higher albedo and the bare sea ice corresponds to the part of lower albedo within plots of low standard deviation. The albedo of the sea ice surface is variable according to the coverage of snow, properties of snow cover (particle size, wet or dry, . . .) and ice (blue or white, . . .) (ISHIKAWA *et al.*, 1982). In this sense, the albedo of 78 may be too high for the average of 100% ice concentration, and a much lower albedo should be chosen. At any rate, the albedo of 100% ice varies greatly owing to the surface condition, and large uncertainties remain in determining the ice concentration from the single-channel albedo.

3.2. Sea ice concentration from two-channel data

Sea ice concentrations are obtained from the albedo of channels 1 and 2 using eq. (1). Albedos of the open water α_i and snow γ_i for two channels are determined from the histogram (Fig. 2) as shown in Section (3.1). The albedos of the bare ice

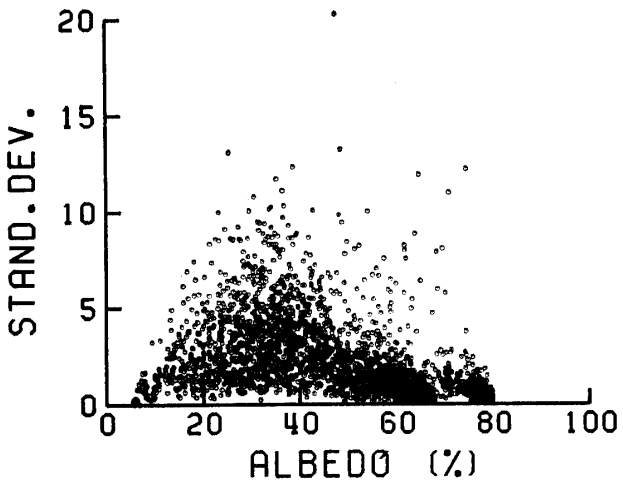

Fig. 4. Local standard deviation against mean albedo of 2×2 array.

β_i are determined from pixels in the bare ice region near the Yamato Mountains (left bottom of Fig. 1). α_i, β_i and γ_i ($i=1, 2$) are shown in Table 1. The albedo for the 100% snow or 100% bare ice does not necessarily correspond to the albedo of the real snow-covered or bare sea ice surface, and the sea ice concentration $y+z$ or the fractional coverage of snow $z/(y+z)$ does not necessarily indicate the absolute value. Moreover, the surface condition of sea ice varies complicatedly and cannot be determined only by the single parameter "the snow coverage". Variation of albedo occurs by the aging of the snow cover, exposing of ice, melting and freezing of the surface

Table 1. Typical albedos of channels 1 and 2 for the open water, bare ice and snow cover (January 29, 1984).

	Channel 1	Channel 2
Open water (α_i)	5%	4%
Bare ice (β_i)	48	27
Snow cover (γ_i)	78	66

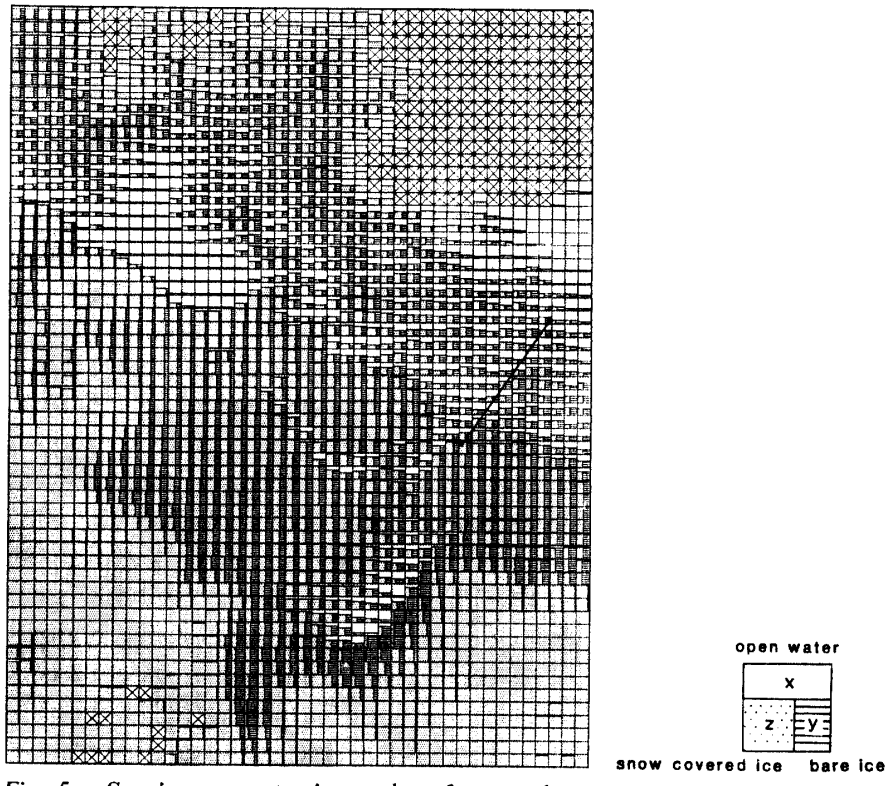

Fig. 5. Sea ice concentration and surface condition map of the research area (January 29, 1984). Dotted area, stripped area and white area in each frame indicate concentration of snow covered ice, bare ice and open water, respectively. So the ordinate of each frame shows the total sea ice concentration and the abscissa (boundary of dotted and stripped areas) shows the surface condition (fractional coverage of snow). The solid line shows a flight route.

snow or ice, and alternation from white ice to blue ice (ISHIKAWA *et al.*, 1982; GRENFEL and PEROVICH, 1984). However, in the present work, the ice surface condition is approximately represented by the single parameter "the snow coverage" just as a simple indicator of surface condition. High $z/(y+z)$ means snow-covered surface and low $z/(y+z)$ means exposed ice.

Figure 5 shows the results for the research area on the same day as in Fig. 3. In this figure, x, y and z are indicated together in each small frame. The open water and the area of low ice concentration can be easily seen. For most of frames in the sea ice region, the ice surface is not covered with 100% snow. Low snow-covered ice is distributed in the southeastern part of Lützow-Holm Bay. In the northwestern part, sea ice is much more covered with snow. Compared with the results by the one-channel data (Fig. 3). the amount of the open water is lower for most frames in this result. The lowering of albedo owing to the change of surface condition was interpreted as the lowering of sea ice concentration in Fig. 3. The result of Fig. 5 is more realistic.

4. Comparison with Photographs Taken by Aircraft

Photographs taken from the helicopter by the 35 mm automatic camera are compared with the satellite data. The flight was made at an altitude of about 200 m aiming an aerial population census of marine animals off Lützow-Holm Bay (NAITO *et al.*, 1986). A part of the flight route on 28 January 1984 is shown by the dotted line in Fig. 1. The target area of each photograph is approximately 125×160 m, with the viewing angle of 30° to the right side of the flight line.

Examples of photographs are shown in Fig. 6. (a) is one for the fast ice. Strong striations, whose direction depends on the privailing wind, are seen within the whole field of view. Surface erosion and melting occurred and some part is covered with snow and some part is exposed. Most of the photographs taken within the fast ice area are the same as this example, and the ice surface condition is between 100% snow cover and bare ice. (b) is a rare example under the flight route in the area of fast ice covered with white snow. Most of the roughness of the surface is smoothed out by snow, leaving only a small number of snow dunes. However, the snow surface itself is different (low albedo) from the continental snow cover used for the 100% extreme in the previous section. (c) is an example where ice floes are crashed into small pieces in the size of about 10 m or less. More than 40% of the field of view is covered with white ice floes and about 30% is covered with sherbet ice. Some region is a newly formed thin ice because sun glitter is seen. (d) includes ice floes covered with white snow and also many small transparent ice floes. Open water is about 50%. The coverage of snow on ice is about 70%, which is larger than the satellite results; however, the white snow may not be the same as the continental snow cover. Since the photograph covers a wide range of the sensitivity from dark open water to bright snow cover, the white part is liable to be saturated and it is difficult by the automated camera and films to distinguish minor ice surface variations. Also, since there is no absolute brightness code for these photographs, it is difficult to discuss the absolute condition of the surface.

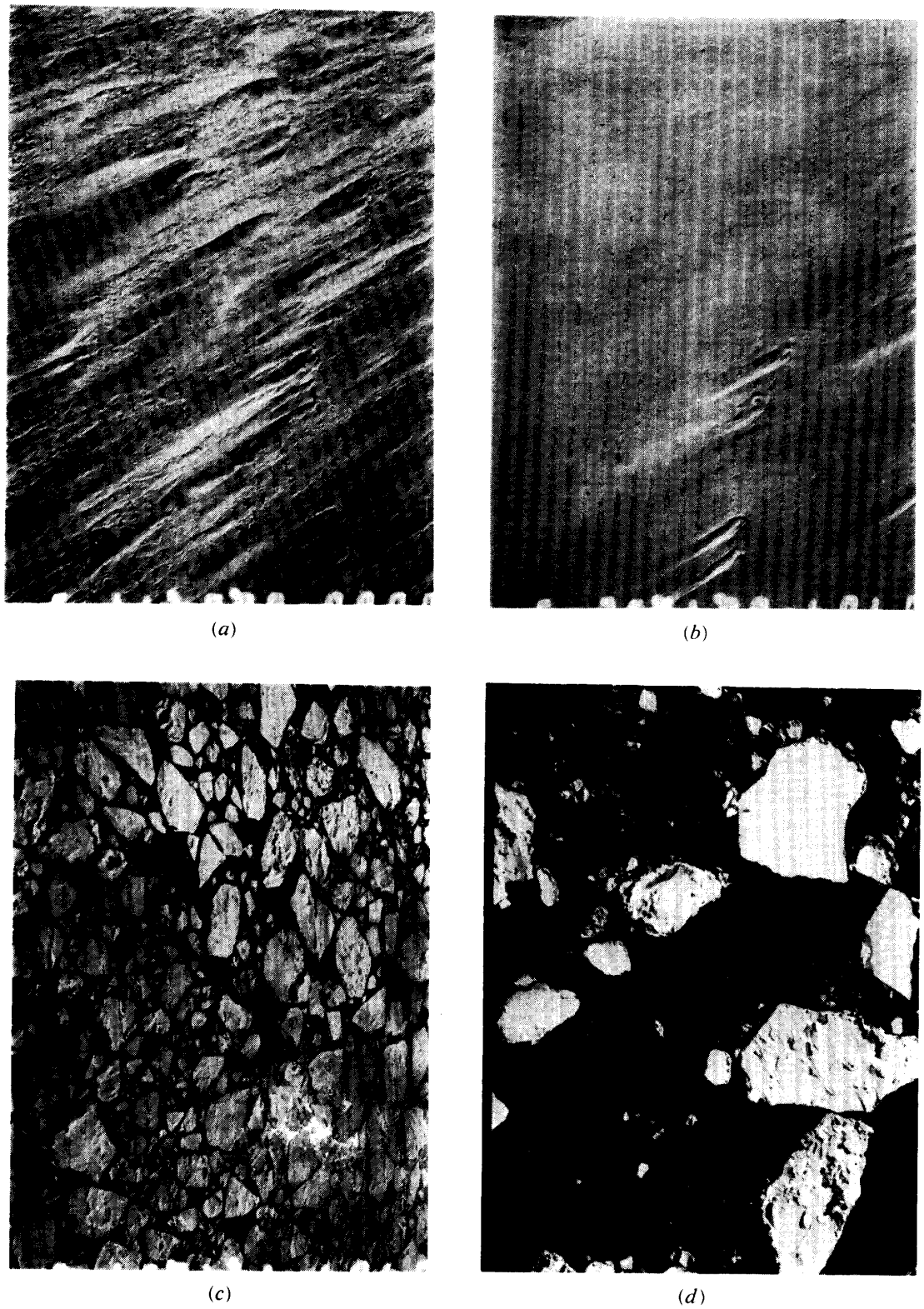

Fig. 6. Air photographs of several types of sea ice along the route shown in Fig. 1 on January 28, 1984. (a) No. 60, (b) No. 109, (c) No. 401 and (d) No. 420.

Ice concentrations are estimated from these photographs sampled each for about 1 km and compared with concentrations derived from the satellite data in Fig. 7. Overall trend of the first 100 photographs (No. 200 to 300) is roughly accompanied by the satellite results; however, in the other part, variations of both the results are out of phase. The disagreement is reasonable considering the time gap of about a day between two observations. Even the sea ice is moving according to the surface wind and ocean current, which is estimated as 15 km/day in average (westerley) off Lützow-Holm Bay (ONO *et al.*, 1986). Another estimate of ice concentration is made from the satellite along the alternative route which starts from the same point and ends at the point 15 km west of the original end point. Then a little improvement of correlation is seen for the latter result. The target area of the air photograph in the order of 100 m is too small to compare with the 1 km resolution of the AVHRR imagery and to represent the area average. Also the positioning of the AVHRR data is difficult even though the affine transformation is conducted and uncertainties of a few km remain.

An atmospheric effect still remains as a future subject. The possibility is mentioned elsewhere that the ice concentration derived by the satellite is liable to be higher than the actual concentration or the satellite albedo is liable to be higher than the albedo assumed from the linear relation of the albedo and the concentration (ONO, 1982). This might be due to the scattering in the atmosphere. The radiation originating from the atmosphere over the dark water is also affected by the radiation reflected from the near by bright ice surface. So, this non-linear relation could result in disagreement between the satellite data and the aircraft data of ice concentration. We first intended to find this relation; however, it was found to be difficult from this ground truth measurements.

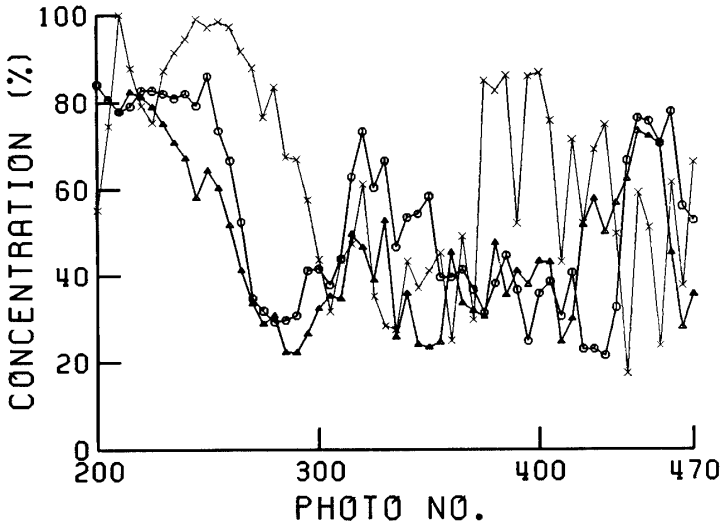

Fig. 7. Comparison of the ice concentration derived from AVHRR data with two channels (circle) and air photograph (cross) along the flight route. Photo number 200 is the start point at the edge of the fast ice and 470 is the end point), and the distance is 93 km. Another estimate of ice concentration from AVHRR along the alternative route which starts from the same point and ends at the point 15 km west of the original end point (triangle).

In order to compare quantitatively, ground truth measurements should be made over a much wider area. The flight should be made at a higher altitude or the flight route should be chosen so as to obtain strip type data of the width of more than 10 km, not the narrow line data. And also measurements should be made simultaneously (with a least time difference) with the satellite pass.

5. Variation of Sea Ice Condition and Concentrations

In order to see the time variation of the sea ice condition and concentrations in summertime, data of other two days with clear sky are analyzed. Results for 14 and 30 December are shown in Figs. 8 and 9, respectively. In Fig. 8, only a small number of frames contain a large part of the open water (called "Otone Lead"), which occurs between the fast ice and the pack ice, and around the east coast of Lützow-Holm Bay. Most part of the fast ice in Lützow-Holm Bay is covered with snow, while the pack ice is not covered with 100% snow. The surface of the pack ice is varied owing to melting or some metamorphosis. Though the percentage is low, many frames in the pack ice region also contain some open water.

Figure 9 shows only a small increase of the number of frames which contain a large part of open water; however, variation of the surface condition for the fast ice region is noticeable. "Snow coverage" on the fast ice decreases to about 60 to 70%. Though the season is a little earlier, the variation is also assumed from the variation of ice surface albedo on the fast ice near Syowa Station reported by ISHIKAWA *et al.* (1982).

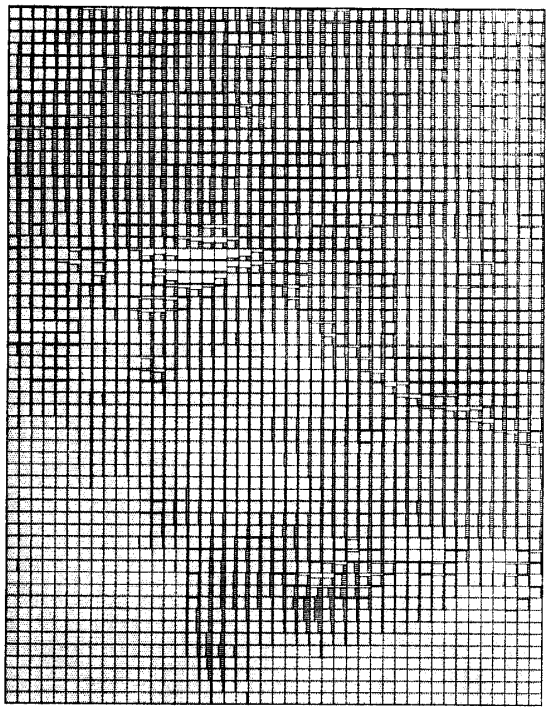

Fig. 8. Sea ice concentration and surface condition distribution map of the research area on December 14, 1983. Other explanation is as Figs. 3 and 5.

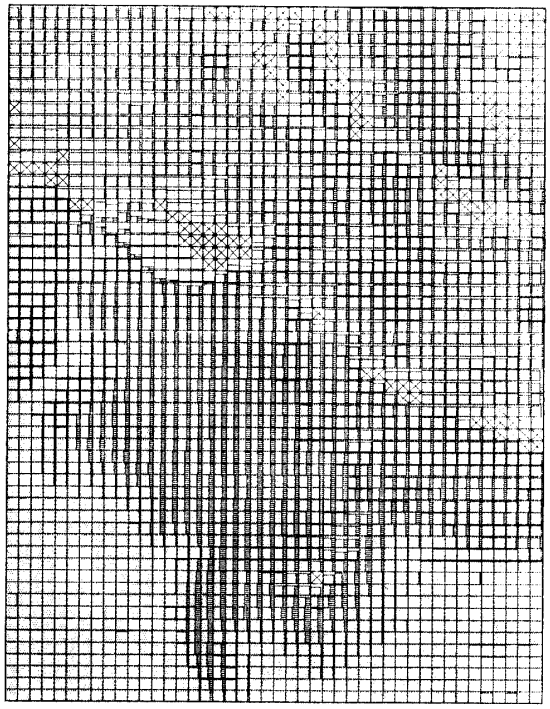

Fig. 9. Same as Fig. 5 but for December 30, 1983.

In Fig. 5, these trends are also enhanced. "Snow coverage" decreases to 30 to 60% except for the fast ice near the west coast of Lützow-Holm Bay. Large region of the open water appears not only in the middle left part near the Riiser-Larsen Peninsula (widening of polynia) but also in the middle right part. Ice concentrations decrease for many frames in the pack ice region.

Variations of the sea ice condition and concentration are also clear in the scatter diagram (Fig. 10) and are shown quantitatively in the two-dimensional histogram in Table 2. On 14 December (Fig. 10a), most of the data points meet around 100% ice concentration and 60 to 100% of snow coverage. On the contrary, on 29 January (Fig. 10c), the points are distributed in a wide range of the concentration and surface condition. However, the distribution of points is restricted to some part and some relation exists between the concentration and the surface condition that there are not so many frames with the high ice concentration and the low snow coverage or that a few frames exist with the low ice concentration and the high snow coverage. From the histogram of Table 2, we can calculate the area of some particular ice concentration and surface condition quantitatively.

6. Concluding Remarks

A new method is proposed to obtain the sea ice concentration using the visible and near infrared albedo of the AVHRR imagery. The method takes into account the variation of albedo of the ice surface (without concentration change), and can derive another indicator of the ice surface condition, which we call "fractional coverage of snow". So, this method can eliminate uncertainties of the ice concentration depending on the variation of only the ice surface condition.

Air photography gives an information of the ice surface condition; however, it does not work efficiently for the quantitative comparison of the ice concentration derived from the satellite data. It is not easy to make a precise ground truth observation. In order to make a quantitative discussion, it is recommended to make a flight at a much higher altitude to get a wider target area and to fly at the same time as the satellite observation.

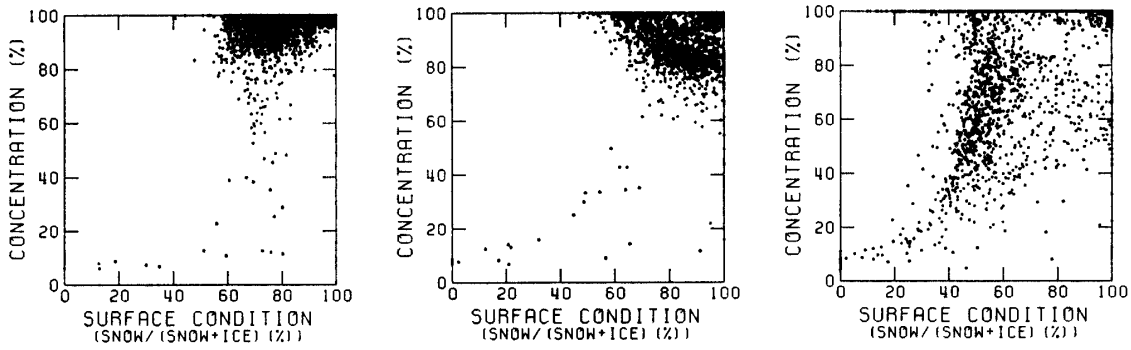

(a) (b) (c)

Fig. 10. Scatter plot of surface condition (snow coverage) versus ice concentration. Each point on the plot represents a small frame of 8×8 array (≈10×10 km) within the research area. (a) December 14, (b) December 30, 1983 and (c) January 29, 1984.

Table 2. Two dimensional histogram of frames of 8×8 array of fractional snow coverage (surface condition) versus ice concentration.

(a) December 14, 1983

Ice concentration (%)	Snow coverage (%) 0–10	–20	–30	–40	–50	–60	–70	–80	–90	–100
90–100	0	0	0	0	2	33	358	565	584	676
90	0	0	0	0	1	13	64	113	43	11
80	0	0	0	0	0	3	12	17	6	2
70	0	0	0	0	0	0	6	11	2	0
60	0	0	0	0	0	0	5	2	0	0
50	0	0	0	0	0	0	0	3	1	0
40	0	0	0	0	0	0	3	1	0	0
30	0	0	0	0	0	1	0	1	1	0
20	0	0	0	0	0	2	0	2	1	1
0– 10	1	3	0	2	0	0	0	0	0	0

(b) December 30, 1983

Ice concentration (%)	Snow coverage (%) 0–10	–20	–30	–40	–50	–60	–70	–80	–90	–100
90–100	0	0	0	0	4	56	306	224	172	619
90	0	0	0	0	0	2	25	153	348	255
80	0	0	0	0	0	0	3	23	68	97
70	0	0	0	0	0	0	0	7	8	17
60	0	0	0	0	0	0	0	0	1	3
50	0	0	0	0	0	1	2	0	0	4
40	0	0	0	0	1	1	2	0	0	0
30	0	0	0	0	2	0	0	0	0	1
20	0	1	2	1	0	0	1	0	0	2
0– 10	11	1	1	0	0	1	0	0	0	0

(c) January 29, 1984

Ice concentration (%)	Snow coverage (%) 0–10	–20	–30	–40	–50	–60	–70	–80	–90	–100
90–100	0	7	13	41	113	200	133	78	79	587
90	0	0	0	5	22	58	35	16	7	3
80	0	0	0	2	15	77	43	15	15	11
70	0	0	0	1	41	66	25	13	12	26
60	0	0	0	4	64	52	9	14	10	23
50	0	0	1	3	49	34	16	7	6	8
40	0	0	1	11	30	18	13	1	0	1
30	0	1	2	10	12	7	0	1	1	2
20	4	3	15	6	1	2	1	1	0	2
0– 10	77	4	1	0	1	0	0	1	0	0

The time variation of the ice concentration and surface condition in summertime is revealed. A noticeable change in ice concentration is seen in the pack ice region and also a great change in the surface condition is found even in the fast ice region.

Acknowledgments

The authors wish to express their sincere thanks to Mr. Y. MAKINO of Meteorological Research Institute (member of the 24th Japanese Antarctic Research Expedition) and crew members of research ship SHIRASE for receiving the satellite data. Thanks are also due to Ms. S. KONDO for typing the manuscript. The processing and analysis of the data were made by utilizing facilities of the Information Processing Center of National Institute of Polar Research including HITAC M-180 system.

References

COMISO, J. C. (1983): Sea ice effective microwave emissivities from satellite passive microwave and infrared observations. J. Geophys. Res., **88**, 7686–7704.

COMISO, J. C. and ZWALLY, H. J. (1982): Antarctic sea ice concentrations inferred from Nimbus 5 ESMR and Landsat imagery. J. Geophys. Res., **87**, 5836–5844.

DEY, B. (1980): Applications of satellite thermal infrared images for monitoring North Water during the periods of polar darkness. J. Glaciol. **25**, 425–438.

DEY, B. (1981): Monitoring winter sea ice dynamics in the Canadian Arctic with NOAA-TIR images. J. Geophys. Res., **86**, 3223–3235.

GRENFELL, T. C. and PEROVICH, D. K. (1984): Spectral albedos of sea ice and incident solar irradiance in the Southern Beaufort Sea. J. Geophys. Res., **89**, 3573–3580.

ISHIKAWA, N., KOBAYASHI, S., OHATA, T. and KAWAGUCHI, S. (1982): Heat balance studies on sea ice near Syowa Station, East Antarctica. Mem. Natl Inst. Polar Res., Spec. Issue, **24**, 234–242.

LEDLEY, T. S. (1985): Sea Ice: Multiyear cycles and white ice. J. Geophys Res., **90**, 5676–5686.

NAITO, Y., HAMADA, Y., TANIGUCHI, A. and YAMANOUCHI T. (1986): Aerial population census conducted off the Lützow-Holm Bay, Antarctica, using a newly developed automatic camera. submitted to Sci. Rep. Whales Res. Inst.

ONO, N. (1982): Interpretation of sea ice in satellite imagery. Mem. Natl Inst. Polar Res., Spec. Issue, **24**, 243–245.

ONO, N., YAMANOUCHI, T., SUZUKI, K. and SHIMIZU, M. (1986): Winter pack ice movements and coastal polynia off Enderby and Queen Maud Lands. submitted to Mem. Natl Inst. Polar Res., Spec. Issue, **44**.

SUZUKI, K., YOSHINO, T., YAMANOUCHI, T., KAWAGUCHI, S. and TANAKA, S. (1985): Extraction of clouds from satellite imagery in the Antarctic (abstract). Mem. Natl Inst. Polar Res., Spec. Issue, **39**, 247.

WARREN, S. G. (1982): Optical properties of snow. Rev. Geophys. Space Phys., **20**, 67–89.

WELLER, G. (1980): Spatial and temporal variations in the south polar surface energy balance. Mon. Weather. Rev. **108**, 2006–2014.

WENDLER, G. (1973): Sea ice observation by means of satellite. J. Geophys. Res., **78**, 1427–1448.

YAMANOUCHI, T. and SEO, Y. (1984): Discrimination of sea ice edge in the Antarcitc, from NOAA MSU. Mem. Natl Inst. Polar Res., Spec. Issue, **34**, 207–217.

(*Received April* 19, 1986; *Revised manuscript received June* 16, 1986)